Springer

KSME

Journal of Mechanical Science and Technology 24 (12) (2010) 2359~2366
www.springerlink.com/content/1738-494x
DOI 10.1007/s12206-010-0924-0

Transverse shear and rotary inertia effects on the stability analysis of functionally graded shells under combined static and periodic axial loadings †

F. Ebrahimi* and H. Sepiani

Department of Mechanical Engineering, University of Tehran, Tehran, Iran

(Manuscript Received May 31, 2009; Revised March 24, 2010; Accepted August 11, 2010)

Abstract

The effect of transverse shear and rotary inertias on the dynamic stability of functionally graded cylindrical shells subjected to combined static and periodic axial forces is investigated in this paper. Material properties of functionally graded cylindrical shells are considered temperature-dependent and are graded in the thickness direction according to a power-law distribution in terms of the volume fractions of the constituents. Numerical results for silicon nitride-nickel cylindrical shells are presented based on two different methods: the first-order shear deformation theory (FSDT) which considers the transverse shear strains and the rotary inertias, and the classical shell theory (CST). The results obtained show that the effect of transverse shear and rotary inertias on the dynamic stability of functionally graded cylindrical shells subjected to combined static and periodic axial forces is dependent on the shell's material composition, environmental temperature, amplitude of static load, deformation mode, and the shell's geometry parameters.

Keywords: Functionally graded material; Dynamic stability; Cylindrical shell

1. Introduction

Functionally graded materials (FGMs) are microscopically inhomogeneous materials. By choosing specific manufacturing processes, the properties of the produced FGMs may vary from point to point or from layer to layer. Most importantly, certain properties (usually the desired ones) of the specifically produced FGMs are superior to those of corresponding homogeneous materials. Recent advances in manufacturing technology have made FGMs more preferential from both functional and economic points of view. As a result, the usage of FGMs has been significantly broadened. For example, there are reports of early successful applications of FGMs used as high-temperature materials in nuclear reactors and chemical plants in Japan [1]. Now, FGMs are also being considered as potential structural materials for future high-speed spacecrafts. Formulation and theoretical analysis of the FGM plates and shells were presented by Reddy [2, 3], Arciniega and Reddy [4], and Praveen et al. [5]. Shell structures composed of this composite material (FGM) also function as basic structural elements used in many engineering structures.

Despite the evident importance in practical applications, investigations on the static and dynamic characteristics of FGM shell structures are still limited in number. Among those available, Loy et al. [6] investigated the free vibration of simply supported FGM cylindrical shells. This investigation was later extended by Pradhan et al. [7] to cylindrical shells under various end supporting conditions. Gong et al. [8] presented an elastic response analysis of simply supported FGM cylindrical shells under low-velocity impact. Ng et al. [9] studied the dynamic instability of simply supported FGM cylindrical shells by using a normal-mode expansion and the Bolotin method to determine the boundaries of the unstable regions. In all the above studies, theoretical formulations were based on the classical shell theory, i.e., neglecting the effect of transverse shear strains. Using Love's shell theory and the Galerkin method, Sofiyev [10] presented an analytic solution for the stability behavior of cylindrical shells made of compositionally (or functionally) graded ceramic–metal materials under axial compressive loads. Also, a solution of the dynamic stability of functionally graded shells under periodic axial loading using the Galerkin procedure was presented by Darabi et al [11], while Matsunaga presented a free vibration and stability analysis of functionally graded circular and shallow shells according to a 2D higher order deformation theory [12, 13]. This paper studies the effect of transverse shear and rotary inertias on the dynamic stability of functionally graded cylindrical shells subjected to combined static and periodic axial forces through a comparison of results obtained by using the following methods: the first-order shear deformation theory

† This paper was recommended for publication in revised form by Associate Editor Seockhyun Kim

* Corresponding author. Tel.: +98 21 88005677, Fax.: +98 21 88013029
E-mail address: febrahimy@ut.ac.ir

(FSDT) which considers transverse shear strains and rotary inertias, and the classical shell theory (CST). Material properties of functionally graded cylindrical shells are considered temperature-dependent and graded in the thickness direction according to a power-law distribution in terms of the volume fractions of the constituents. The results show that the effect of transverse shear and rotary inertias on the dynamic stability of functionally graded cylindrical shells subjected to combined static and periodic axial forces is dependent on the shell's material composition, environmental temperature, amplitude of static load, deformation mode, and the shell's geometry parameters. It is found that the effect of transverse shear and rotary inertias on the dynamic stability of functionally graded cylindrical shells subjected to combined static and periodic axial forces cannot be neglected. The new features of the effect of transverse shear and rotary inertias on the dynamic stability of functionally graded cylindrical shells and the results in this paper are helpful for the application and design of nuclear reactors, spacecraft, and chemical plants, in which functionally graded cylindrical shells act as basic elements.

2. Theoretical formulations

An FGM cylindrical shell with mean radius of *R,* thickness *h,* and length *L* is shown in Fig. 1. The displacement components in the *x,* θ , and *z* directions are denoted by *u, v*, and *w*, respectively. The pulsating axial load is given by

$$N_a = N_o + N_d \cos Pt\,, \tag{1}$$

where *P* is the frequency of excitation in radians per unit time.

The temperature and position-dependent material properties of FGM cylindrical shells are accurately modeled by using a simple rule of mixtures for the stiffness parameters coupled with the temperature-dependent properties of the constituents. The volume fraction is described by a spatial function as follows:

$$V(z) = (z/h + 1/2)^{\Phi}\,, \quad (0 \le \Phi \le \infty)\,, \tag{2}$$

where Φ expresses the volume fraction exponent. The combination of these functions gives rise to the effective properties of functionally graded materials. An FGM cylindrical shell that is metal-rich at the inner surface and ceramic-rich at the outer surface is defined as Type A. The corresponding effective material properties are expressed as

$$F_{eff}(T,z) = F_c(T)V(z) + F_m(T)\big(1 - V(z)\big)\,, \tag{3}$$

where F_{eff} is the effective material property of the FGM cylindrical shell, including the effective elastic modulus, effective mass density, and effective Poisson's ratio. F_c and F_m are the temperature-dependent properties of the ceramic and metal, respectively. On the other hand, an FGM cylindrical shell that is ceramic-rich at the inner surface and metal-rich at the outer surface is defined as Type B, whose effective material properties are given by

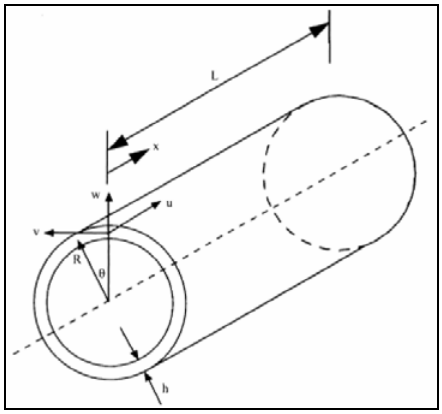

Fig. 1. Coordinate system of the FGM cylindrical shell.

$$F_{eff}(T,z) = F_m(T)V(z) + F_c(T)\big(1 - V(z)\big)\,. \tag{4}$$

Based on the first-order shear deformation theory (FSDT), the equations of motion for an FGM cylindrical shell under axially dynamic load are as follows [10, 14]:

$$\frac{\partial N_1}{\partial x} + \frac{1}{R}\frac{\partial N_6}{\partial \theta} = I_1 u'' + I_2 \phi_1'' \tag{5}$$

$$\frac{\partial N_6}{\partial x} + \frac{1}{R}\frac{\partial N_1}{\partial \theta} + \frac{1}{R}Q_2 + N_a\frac{\partial^2 v}{\partial x^2} = I_1 v'' + I_2 \phi_2'' \tag{6}$$

$$\frac{\partial Q_1}{\partial x} + \frac{1}{R}\frac{\partial Q_2}{\partial \theta} - \frac{N_2}{R} + N_a\frac{\partial^2 w}{\partial x^2} = I_1 w'' \tag{7}$$

$$\frac{\partial M_1}{\partial x} + \frac{1}{R}\frac{\partial M_6}{\partial \theta} - Q_1 = I_2 u'' + I_3 \phi_1'' \tag{8}$$

$$\frac{\partial M_6}{\partial x} + \frac{1}{R}\frac{\partial M_2}{\partial \theta} - Q_2 = I_2 v'' + I_3 \phi_2'' \tag{9}$$

where ϕ_1 and ϕ_2 are the rotations of a normal to the reference surface, $I_i (i = 1,2,3)$ is the mass inertia terms defined as

$$(I_1, I_2, I_3) = \int_{-\frac{h}{2}}^{\frac{h}{2}} \rho(z)(1, z, z^2)dz\,, \tag{10}$$

and $\rho(z)$ is the effective mass density of functionally graded materials.

The stress resultants of FGM cylindrical shells are given by

$$\begin{pmatrix} N_1 \\ N_2 \\ N_6 \\ M_1 \\ M_2 \\ M_6 \end{pmatrix} = \begin{pmatrix} A_{11} & A_{12} & 0 & B_{11} & B_{12} & 0 \\ A_{21} & A_{22} & 0 & B_{21} & B_{22} & 0 \\ 0 & 0 & A_{66} & 0 & 0 & B_{66} \\ B_{11} & B_{12} & 0 & D_{11} & D_{12} & 0 \\ B_{21} & B_{22} & 0 & D_{21} & D_{22} & 0 \\ 0 & 0 & B_{66} & 0 & 0 & D_{66} \end{pmatrix} \begin{pmatrix} \varepsilon_1 \\ \varepsilon_2 \\ \varepsilon_6 \\ \kappa_1 \\ \kappa_2 \\ \kappa_6 \end{pmatrix}$$

$$\begin{pmatrix} Q_1 \\ Q_2 \end{pmatrix} = = \begin{pmatrix} C_{44} & 0 \\ 0 & C_{55} \end{pmatrix} \begin{pmatrix} \varepsilon_5 \\ \varepsilon_4 \end{pmatrix} \tag{11}$$

where A_{ij}, B_{ij}, D_{ij} and C_{ij} are, respectively, the extensional, coupling, bending, and shear stiffness. These are given by

$$\left(A_{ij},B_{ij},D_{ij}\right)=\int_{-\frac{h}{2}}^{\frac{h}{2}}Q_{ij}(1,z,z^2)dz\,,\quad (i,j=1,2,6)$$

$$Q_{11}=Q_{22}=\frac{E_{eff}}{1-\nu_{eff}{}^2}\qquad C_{44}=\int_{-\frac{h}{2}}^{\frac{h}{2}}Q_{44}\,dz$$

$$Q_{12}=Q_{21}=\frac{\nu_{eff}E_{eff}}{A(1-\nu_{eff}{}^2)}\qquad C_{55}=\int_{-\frac{h}{2}}^{\frac{h}{2}}Q_{55}\,dz$$

$$Q_{44}=\kappa\frac{E_{eff}}{2\left(1+\nu_{eff}\right)}\qquad Q_{66}=\frac{E_{eff}}{2A(1+\nu_{eff})}\qquad (12)$$

$$Q_{55}=Q_{44}/A\qquad A=1+z/R$$

where E_{eff} and ν_{eff}. are the effective elastic modulus and effective Poisson's ratio of FGM cylindrical shells, respectively. κ is the shear correction factor introduced by Reddy [2] and is equal to 5/6. The strains are expressed as

$$\varepsilon_1=\frac{\partial u}{\partial x}\,,\qquad \varepsilon_2=\frac{1}{R}\left(\frac{\partial v}{\partial\theta}+w\right)\,,$$

$$\varepsilon_6=\frac{\partial v}{\partial x}+\frac{1}{R}\frac{\partial u}{\partial\theta},\qquad \varepsilon_4=\phi_2+\frac{1}{R}\frac{\partial w}{\partial\theta},$$

$$\varepsilon_5=\phi_1+\frac{\partial w}{\partial x}\quad,\qquad \kappa_1=\frac{\partial\phi_1}{\partial x},$$

$$\kappa_2=\frac{1}{R}\frac{\partial\phi_2}{\partial\theta}\quad,\qquad \kappa_6=\frac{\partial\phi_2}{\partial x}+\frac{1}{R}\frac{\partial\phi_1}{\partial\theta}\qquad (13)$$

Utilizing Eqs. (5-9), (11) and (13), the equations of motion can be expressed in terms of generalized displacement (u,v,w,ϕ_1,ϕ_2) as follows:

$$L_1(u,v,w,\phi_1,\phi_2)=I_1u''+I_2\phi_1''\qquad (14)$$

$$L_2(u,v,w,\phi_1,\phi_2)+N_a\frac{\partial^2v}{\partial x^2}=I_1v''+I_2\phi_2''\qquad (15)$$

$$L_3(u,v,w,\phi_1,\phi_2)+N_a\frac{\partial^2w}{\partial x^2}=I_1w''\qquad (16)$$

$$L_4(u,v,w,\phi_1,\phi_2)=I_2u''+I_3\phi_1''\qquad (17)$$

$$L_5(u,v,w,\phi_1,\phi_2)=I_2v''+I_3\phi_2''\qquad (18)$$

By neglecting terms I_2 and I_3 involved in Eqs. (5-9) and setting

$$\phi_1=-\frac{\partial w}{\partial x},\qquad \phi_2=-\frac{1}{R}\frac{\partial w}{\partial\theta},\qquad (19)$$

the equations of motion based on a classical shell theory (CST) can be easily obtained.

Here, the two ends of the FGM cylindrical shells are considered simply supported, so a solution for the motion equations (14-18) can be described by

$$\begin{aligned}
u_{mn}&=\bar{A}_{mn}e^{i\omega t}\cos\lambda_m\ x\cos n\theta\\
v_{mn}&=\bar{B}_{mn}e^{i\omega t}\sin\lambda_m\ x\sin n\theta\\
w_{mn}&=\bar{C}_{mn}e^{i\omega t}\sin\lambda_m\ x\cos n\theta\\
\phi_{1mn}&=\bar{H}_{mn}e^{i\omega t}\cos\lambda_m\ x\cos n\theta\\
\phi_{2mn}&=\bar{K}_{mn}e^{i\omega t}\sin\lambda_m\ x\sin n\theta
\end{aligned}\qquad (20)$$

where $\lambda_m=\dfrac{m\pi}{L}$., n represents the number of circumferential waves, and m represents the number of axial half-waves.

Substituting Eq. (20) into Eqs. (14-18) and letting $N_d=0$ in Eq. (1) yields

$$\left(\begin{bmatrix}T_{11}&T_{12}&T_{13}&T_{14}&T_{15}\\T_{21}&T_{12}+\lambda_m^2N_0&T_{23}&T_{24}&T_{25}\\T_{31}&T_{31}&T_{33}+\lambda_m^2N_0&T_{34}&T_{35}\\T_{41}&T_{42}&T_{43}&T_{44}&T_{45}\\T_{51}&T_{52}&T_{53}&T_{54}&T_{55}\end{bmatrix}-\omega^2\begin{bmatrix}I_1&0&0&I_2&0\\0&I_1&0&0&I_2\\0&0&I_1&0&0\\I_2&0&0&I_3&0\\0&I_2&0&0&I_3\end{bmatrix}\right)\begin{Bmatrix}\bar{A}_{mn}\\\bar{B}_{mn}\\\bar{C}_{mn}\\\bar{H}_{mn}\\\bar{K}_{mn}\end{Bmatrix}=\begin{Bmatrix}0\\0\\0\\0\\0\end{Bmatrix}\qquad (21)$$

where T_{ij} is given in Appendix A.

To solve the equations of motion containing the dynamic load N_d, a solution is sought in the form shown below:

$$u=\sum_{j=1}^{5}\sum_{m=1}^{\infty}\sum_{n=1}^{\infty}q_{mnj}(t)U_{mnj}(x,\theta)=\sum_{j=1}^{5}\sum_{m=1}^{\infty}\sum_{n=1}^{\infty}q_{mnj}(t)\bar{A}_{mnj}\cos\lambda_m\ x\cos n\theta\qquad (22)$$

$$v=\sum_{j=1}^{5}\sum_{m=1}^{\infty}\sum_{n=1}^{\infty}q_{mnj}(t)V_{mnj}(x,\theta)=\sum_{j=1}^{5}\sum_{m=1}^{\infty}\sum_{n=1}^{\infty}q_{mnj}(t)\bar{B}_{mnj}\sin\lambda_m\ x\sin n\theta\qquad (23)$$

$$w=\sum_{j=1}^{5}\sum_{m=1}^{\infty}\sum_{n=1}^{\infty}q_{mnj}(t)W_{mnj}(x,\theta)=\sum_{j=1}^{5}\sum_{m=1}^{\infty}\sum_{n=1}^{\infty}q_{mnj}(t)\bar{C}_{mnj}\sin\lambda_m\ x\cos n\theta\qquad (24)$$

$$\phi_1=\sum_{j=1}^{5}\sum_{m=1}^{\infty}\sum_{n=1}^{\infty}q_{mnj}(t)\theta_{xmnj}(x,\theta)=\sum_{j=1}^{5}\sum_{m=1}^{\infty}\sum_{n=1}^{\infty}q_{mnj}(t)\bar{H}_{mnj}\cos\lambda_m\ x\cos n\theta\qquad (25)$$

$$\phi_2=\sum_{j=1}^{5}\sum_{m=1}^{\infty}\sum_{n=1}^{\infty}q_{mnj}(t)\theta_{\theta mnj}(x,\theta)=\sum_{j=1}^{5}\sum_{m=1}^{\infty}\sum_{n=1}^{\infty}q_{mnj}(t)\bar{K}_{mnj}\sin\lambda_m\ x\sin n\theta\qquad (26)$$

where $q_{mnj}(t)$ is a generalized co-ordinate and U_{mnj}, V_{mnj}, W_{mnj}, θ_{xmnj}, and $\theta_{\theta mnj}$. are the modal functions of FGM cylindrical shells with simply supported ends under the axially static load N_0. Substituting Eqs. (22-26) into Eqs. (14-18), yields

$$L_1(U_{mnj},V_{mnj},W_{mnj},\theta_{xmnj},\theta_{\theta mnj})=-I_1\omega_{mnj}^2U_{mnj}-I_2\omega_{mnj}^2H_{mnj}\qquad (27)$$

$$L_2(U_{mnj},V_{mnj},W_{mnj},\theta_{xmnj},\theta_{\theta mnj})-N_0\lambda_m^2V_{mnj}=-I_1\omega_{mnj}^2V_{mnj}-I_2\omega_{mnj}^2\theta_{\theta mnj}\qquad (28)$$

$$L_3(U_{mnj},V_{mnj},W_{mnj},\theta_{xmnj},\theta_{\theta mnj})-N_0\lambda_m^2W_{mnj}=-I_1\omega_{mnj}^2W_{mnj}\qquad (29)$$

$$L_4(U_{mnj},V_{mnj},W_{mnj},\theta_{xmnj},\theta_{\theta mnj})=-I_2\omega_{mnj}^2U_{mnj}-I_3\theta_{xmnj}\qquad (30)$$

$$L_5(U_{mnj},V_{mnj},W_{mnj},\theta_{xmnj},\theta_{\theta mnj})=-I_2\omega_{mnj}^2V_{mnj}-I_3\theta_{\theta mnj}\qquad (31)$$

Eqs. (14-18) may be rewritten as

$$\sum_{j=1}^{5}\sum_{m=1}^{\infty}\sum_{n=1}^{\infty}\left(q_{mnj}''+\omega_{mnj}^2q_{mnj}\right)\left(I_1A_{mnj}+I_2H_{mnj}\right)\cos\lambda_m\ x\cos n\theta=0\qquad (32)$$

$$\sum_{j=1}^{5}\sum_{m=1}^{\infty}\sum_{n=1}^{\infty}\left(q''_{mnj}+\omega^2_{mnj}q_{mnj}\right)\left(I_1B_{mnj}+I_2K_{mnj}\right)\sin\lambda_m\ x\sin n\theta$$
$$+N_d\cos Pt\sum_{j=1}^{5}\sum_{m=1}^{\infty}\sum_{n=1}^{\infty}\lambda_m^2B_{mnj}q_{mnj}\sin\lambda_m\ x\sin n\theta=0 \quad (33)$$

$$\sum_{j=1}^{5}\sum_{m=1}^{\infty}\sum_{n=1}^{\infty}\left(q''_{mnj}+\omega^2_{mnj}q_{mnj}\right)I_1C_{mnj}\sin\lambda_m\ x\cos n\theta$$
$$+N_d\cos Pt\sum_{j=1}^{5}\sum_{m=1}^{\infty}\sum_{n=1}^{\infty}\lambda_m^2C_{mnj}q_{mnj}\sin\lambda_m\ x\cos n\theta=0 \quad (34)$$

$$\sum_{j=1}^{5}\sum_{m=1}^{\infty}\sum_{n=1}^{\infty}\left(q''_{mnj}+\omega^2_{mnj}q_{mnj}\right)\left(I_2A_{mnj}+I_3H_{mnj}\right)\cos\lambda_m\ x\cos n\theta=0 \quad (35)$$

$$\sum_{j=1}^{5}\sum_{m=1}^{\infty}\sum_{n=1}^{\infty}\left(q''_{mnj}+\omega^2_{mnj}q_{mnj}\right)\left(I_2B_{mnj}+I_3K_{mnj}\right)\sin\lambda_m\ x\sin n\theta=0 \quad (36)$$

Making use of the orthogonality condition, Eqs. (32-36) are simplified to

$$\begin{bmatrix} m_1 & 0 & 0 & 0\\ 0 & m_1 & 0 & 0\\ 0 & 0 & \mathrm{O} & 0\\ 0 & 0 & 0 & m_{5N^2}\end{bmatrix}\begin{Bmatrix} q''_1\\ q''_2\\ M\\ q''_{5N^2}\end{Bmatrix}+$$
$$\left(\begin{bmatrix} k_1 & 0 & 0 & 0\\ 0 & k_2 & 0 & 0\\ 0 & 0 & \mathrm{O} & 0\\ 0 & 0 & 0 & k_{5N^2}\end{bmatrix}-N_d\cos Pt\begin{bmatrix} \bar{Q}_1 & 0 & 0 & 0\\ 0 & \bar{Q}_2 & 0 & 0\\ 0 & 0 & \mathrm{O} & 0\\ 0 & 0 & 0 & \bar{Q}_{5N^2}\end{bmatrix}\right)\begin{Bmatrix} q_1\\ q_2\\ M\\ q_{5N^2}\end{Bmatrix}=0 \quad (37)$$

where

$$m_I=\frac{\pi l}{2}\left[\left(I_1\bar{B}_I+I_2\bar{K}_I\right)^2+\left(I_1\bar{A}_I+I_2\bar{H}_I\right)^2+\left(I_1\bar{C}_I\right)^2+\left(I_2\bar{A}_I+I_3\bar{H}_I\right)^2+\left(I_2\bar{B}_I+I_3\bar{K}_I\right)^2\right]$$
$$k_I=\omega_I^2m_I,\quad \bar{Q}_I=-\frac{\pi L}{2}\lambda_m^2\left[\bar{B}_I\left(I_1\bar{B}_I+I_2\bar{K}_I\right)+I_1\bar{C}_I{}^2\right] \quad (38)$$

$$(m,n)=(1,1):\ I=1(j=1),\ 2(j=2),\ 3(j=3),\ 4(j=4),\ 5(j=5);$$
$$(m,n)=(1,2):\ I=6(j=1),\ 7(j=2),\ 8(j=3),\ 9(j=4),\ 10(j=5);$$

$$(m,n)=(1,N):\ I=5(N-4)\,(j=1),\ 5(N-3)\,(j=2),\ 5N\,(j=5);$$
$$(m,n)=(2,1):\ I=5N+1\,(j=1),\ 5N+2\,(j=2),\ 5N+5\,(j=5);$$

$$(m,n)=(N,N):\ I=5N^2-4\,(j=1),\ 5N^2-3\,(j=2),\ 5N^2\,(j=5); \quad (39)$$

In the above formula, the coefficients of mode shapes $\bar{A}_I$, $\bar{B}_I$, $\bar{C}_I$, $\bar{H}_I$ and $\bar{K}_I$ can be obtained from Eq. (21).

Based CST and the orthogonality condition, Eq. (37) can be simplified to

$$\begin{bmatrix} m_1 & 0 & 0 & 0\\ 0 & m_1 & 0 & 0\\ 0 & 0 & \mathrm{O} & 0\\ 0 & 0 & 0 & m_{3N^2}\end{bmatrix}\begin{Bmatrix} q''_1\\ q''_2\\ M\\ q''_{3N^2}\end{Bmatrix}+$$
$$\left(\begin{bmatrix} k_1 & 0 & 0 & 0\\ 0 & k_2 & 0 & 0\\ 0 & 0 & \mathrm{O} & 0\\ 0 & 0 & 0 & k_{3N^2}\end{bmatrix}-N_d\cos Pt\begin{bmatrix} \bar{Q}_1 & 0 & 0 & 0\\ 0 & \bar{Q}_2 & 0 & 0\\ 0 & 0 & \mathrm{O} & 0\\ 0 & 0 & 0 & \bar{Q}_{3N^2}\end{bmatrix}\right)\begin{Bmatrix} q_1\\ q_2\\ M\\ q_{3N^2}\end{Bmatrix}=\begin{Bmatrix} 0\\ 0\\ M\\ 0\end{Bmatrix} \quad (40)$$

where

$$m_I=\frac{\pi l}{2}\left[\left(I_1\bar{B}_I\right)^2+\left(I_1\bar{A}_I\right)^2+\left(I_1\bar{C}_I\right)^2\right],\qquad k_I=\omega_I^2m_I,$$
$$\bar{Q}_I=-\frac{\pi L}{2}\lambda_m^2\left[\bar{B}_I\left(I_1\bar{B}_I\right)+I_1\bar{C}_I{}^2\right],\quad I=1,2,3,...,3N^2 \quad (41)$$

The coefficients $\bar{A}_I$, $\bar{B}_I$, $\bar{C}_I$ in Eq. (40) can be obtained from Eq. (24).

Eqs. (37) and (40) are in the form of second order differential equations with periodic coefficients of the Mathieu-Hill type. Using the method presented by Bolotin [15], the regions of unstable solutions are separated by periodic solutions. As a first approximation, the periodic solutions with period $2T$ can be sought in the form

$$q_I=a_I\sin\frac{Pt}{2}+b_I\cos\frac{Pt}{2} \quad (42)$$

where a_I and b_I are arbitrary constants.

By substituting Eq. (42) into Eqs. (37) and (40) and equating the coefficients of the $\sin Pt/2$ and $\cos Pt/2$ terms, a set of linear homogeneous algebraic equations in terms of a_I and b_I can be obtained. The conditions for non-trivial solutions for the linear homogeneous algebraic equations are

$$-\frac{1}{4}\bar{P}_I^2m_I+k_I-\frac{1}{2}N_d\bar{Q}_I=0 \quad (43)$$
$$-\frac{1}{4}\bar{P}_I^2m_I+k_I+\frac{1}{2}N_d\bar{Q}_I=0 \quad (44)$$

Each unstable region is bounded by two lines which originate from a common point from the P-axis. The branches emanate at $N_d=0$ from $2\omega_I$. The left and right branch correspond with

$$\bar{P}_I=\sqrt{\frac{4k_I+2N_d\bar{Q}_I}{m_I}}\quad and\quad \bar{P}_I=\sqrt{\frac{4k_I-2N_d\bar{Q}_I}{m_I}}\quad (N_d>0)$$

or

$$\bar{P}_I=\sqrt{\frac{4k_I-2N_d\bar{Q}_I}{m_I}}\quad and\quad \bar{P}_I=\sqrt{\frac{4k_I+2N_d\bar{Q}_I}{m_I}}\quad (N_d<0).$$

3. Numerical results and discussions

The ceramic material used in this study is silicon nitride and the metal material used is nickel [9]. The density of silicon

Table 1. Comparison of the point of origin P_1 for a simply supported silicon nitride-nickel FGM cylindrical shell under axial extensional loading.

	P_1 (Type A)		P_1 (Type B)	
	Present	Ng et al.[9]	Present	Ng et al.[9]
0	10.955	10.956	10.778	10.774
0.5	10.896	10.894	10.849	10.849
1.0	10.867	10.865	10.883	10.883
5.0	10.809	10.805	10.936	10.937
10	10.795	10.791	10.945	10.946
∞	10.778	10.773	10.955	10.946

nitride is ρ_c =2370 kg/m^{3}and that of nickel is ρ_m =8900 kg/m^3, while the Poisson's ratio is ν_c =0.24 for silicon nitride and ν_m =0.31 for nickel. These are independent of temperature. The elastic moduli are temperature-dependent and are obtained from Ng et al. [9] as

$$E_c = 348.43\times10^9\left(1-3.070\times10^{-4}T+2.160\times10^{-7}T^2-8.946\times10^{-11}T^3\right)$$
$$E_m = 223.95\times10^9\left(1-2.794\times10^{-4}T-3.998\times10^{-9}T^2\right)$$

where E_c and E_m are the elastic moduli (in Pa) of silicon nitride and nickel, respectively, and T is the temperature (in Kelvin). The elastic moduli E_c and E_m are substituted into F_c and F_m in Eq. (3) respectively in order to compute the effective elastic moduli of the FGM shell.

3.1 Comparison studies

Example. Based on CST, the point of origin, $P_1 = 2\times\omega_1\times\alpha$ [the nondimensionalized coefficient $\alpha = 2\pi R\times\sqrt{I_1/A_{11}}$, $I=1$, see Eq. (39)] is presented in Table 1 for a silicon nitride-nickel FGM cylindrical shell with simply supported ends under axial extensional loading. The computation parameters are taken as $m=n=1$, $N_0=0.5N_{cr}$, $L/R=1$, $R/h=100$.

The results in Table 1 present the transverse modes corresponding to the point of origin P_1, and are in a good agreement with Ng et al. [9].

3.2 Parametric resonance results

The dynamic instability regions for the first order parametric resonances of a silicon nitride-nickel FGM (Type A) cylindrical shell with simply supported ends under combined static and periodic axial loads are presented in Fig. 2 using CST and FSDT. The effect of FSDT on the dynamic instability regions is related to the points of origin $P_1=2\times\omega_6\times\alpha\,(I=6)$, $P_2=2\times\omega_{16}\times\alpha\,(I=16)$, and $P_3=2\times\omega_1\times\alpha\,(I=1)$ (see Eq. (39), FSDT). For the points P_1 and P_2, the dynamic instability regions obtained from FSDT are less than those obtained from the CST, not considering shear deformation and rotary inertias. For the point P_3, the dynamic instability regions are

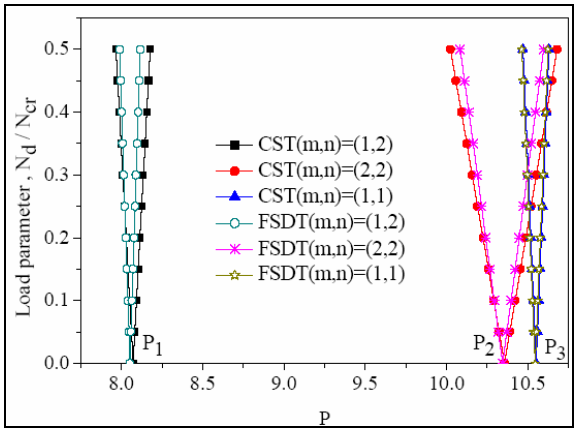

Fig. 2. Comparison of classical shell theory and first-order shear deformation theory unstable regions for a simply supported silicon nitride-nickel FGM Type A cylindrical shell under combined static axial compressive loading and periodic axial loading (m=1,2, n=1,2, $N_0=0.5N_{cr}$, L/R=1.0, T=300K, Φ=1.0, h/R=0.01).

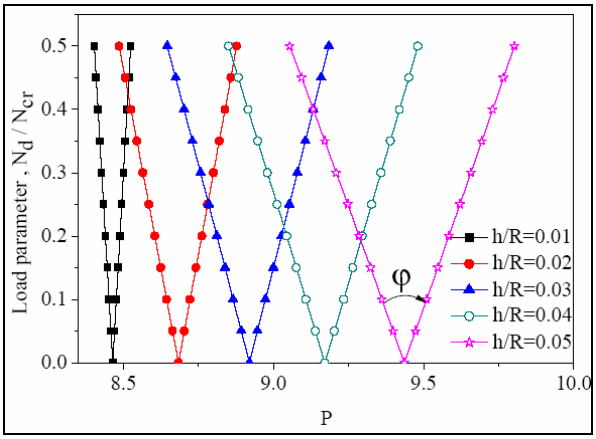

Fig. 3. Effect of thickness to radius ratio h/R on the first unstable region (corresponding to the points of origin 1 P_1) for a simply supported silicon nitride-nickel FGM Type A cylindrical shell under combined static axial extensional loading and periodic axial load (m=1,2, n=1,2, $N_0=0.5N_{cr}$, L/R=1.0, T=300K, Φ=1.0).

very close for CST and FSDT, where ω_6, ω_{16} and ω_1 denote the three lowest natural frequency using FSDT.

Fig. 3 shows the effect of thickness to radius ratio (h/R) on the first unstable region (corresponding to the point of origin P_1) for a silicon nitride-nickel FGM cylindrical shell under combined static axial extensional loading and periodic axial load based on FSDT. It is observed that the points of origin of the unstable region are lower for the thinner shells. The angle φ gives a good measure of the size of the unstable region in Fig. 3. Here, the unstable regions increase with increasing thicknesses.

The effect of static axial compressive loading N_o/N_{cr} on unstable angles φ can be seen from the results presented in Fig. 4 using CST and FSDT. The points of origin are, respectively, $P_1=2\times\omega_6\times\alpha\,(I=6)$, $P_2=2\times\omega_{16}\times\alpha\,(I=16)$, $P_3=2\times\omega_1\times\alpha\,(I=1)$, and $P_4=2\times\omega_{11}\times\alpha\,(I=11)$ (see Eq.

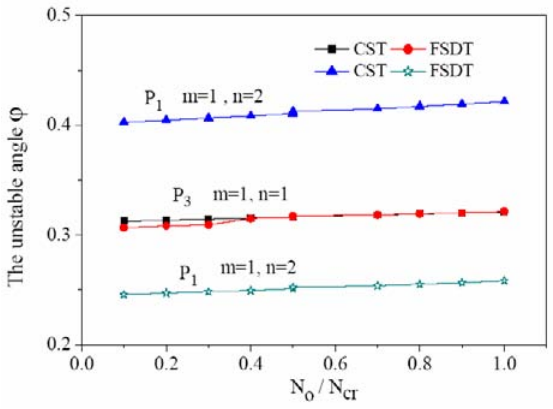

(a)

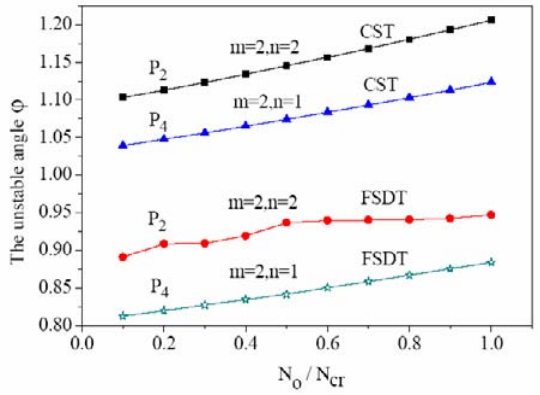

(b)

Fig. 4. Unstable region φ versus axial compressive loading N_0/N_{cr} for a simply supported silicon nitride-nickel FGM Type A cylindrical shell under combined static axial compressive loading and periodic axial loading (m=1,2, n=1,2, L/R=1.0, T=300K, Φ=1.0 , h/R=0.01).

(39), FSDT). The first four unstable angles φ (corresponding to the points of origin P_1 , P_2 , P_3 , P_4) for a silicon nitride-nickel FGM cylindrical shell under combined static axial compressive loading and periodic axial loading are described in Fig. 4(a) and Fig. 4(b), respectively. The unstable region increases as the static axial load increases, and the effect of shear deformation and rotary inertias on the unstable region is dependent on the points of origin. It is shown from the results presented in Figs. 4(a) and (b) that the unstable angles for the points P_1 , P_2 and P_4 obtained using FSDT are less than those obtained using CST, and when the static axial compressive loading N_o/N_{cr} is larger than 0.4, the third unstable angle (corresponding to the point of origin P_3 and m=1, n=1) is almost the same using CST and FSDT.

Figs. 5(a-c) show the effect of the volume fraction exponent on the unstable angle φ of a silicon nitride-nickel FGM cylindrical shell under combined static axial compressive loading and periodic axial loading based on CST and FSDT. The first three unstable regions (corresponding to the points of origin P_1 , P_2 and P_3) are described in Figs. 5(a-c), respectively. It is observed that the unstable angle φ nonlinearly

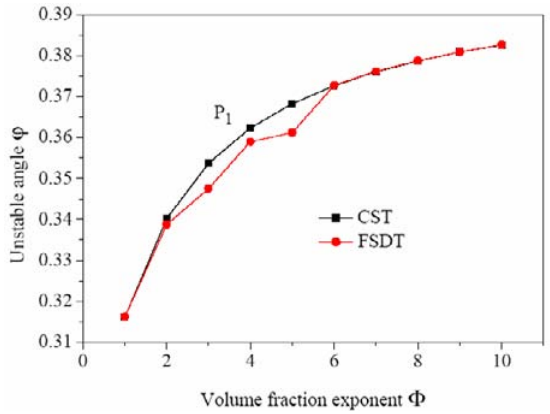

(a)

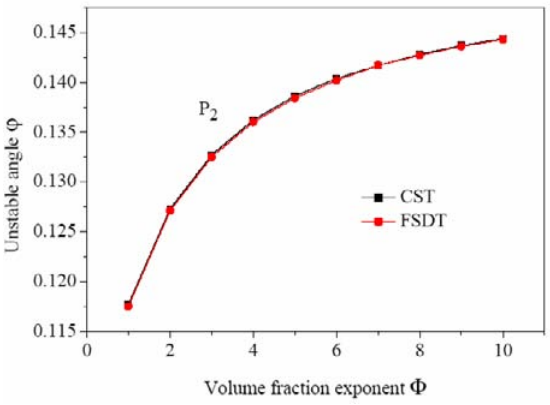

(b)

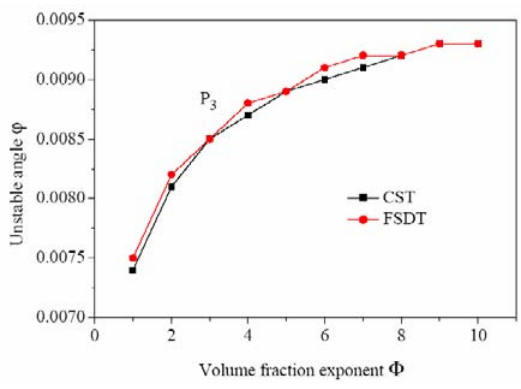

(c)

Fig. 5. Effect of the volume fraction exponent Φ on the unstable angles φ for a simply supported silicon nitride-nickel FGM Type A cylindrical shell under combined static axial compressive loading and periodic axial loading (m=1 , n=1, $N_0 = 0.5N_{cr}$, L/R=1.0, T=300K, Φ=1.0 , h/R=0.01).

increases as the volume fraction exponent Φ increases, the effect of shear deformation and rotary inertias on the unstable angles (corresponding to m=1, n=1) is not only dependent on the points of origin but also on the volume fraction exponent Φ , and the unstable angles for the point P_2 obtained by using CST and FSDT are the same.

4. Conclusions

This paper reports the result of an investigation into the effect of the first-order shear deformation theory considering rotary inertia and the transverse shear strains on the dynamic instability of functionally graded cylindrical shells with simply-supported ends, under combined static and periodic axial forces. The result obtained using the first-order shear deformation theory (FSDT) is compared with that obtained using classical shell theory (CST). The differences between the results from FSDT and the results from CST increase as the deformation mode and thickness increase. It was found that reasonable control can be achieved on the dynamic instability regions by correctly varying the ratio of length to radius, the ratio of thickness to radius, the amplitude of static axial load, thermal environment, and the volume fraction exponent.

Nomenclature

A,B,D,C : Extensional, coupling, bending and shear stiffness, respectively
E : Elastic modulus
F : Material property
H : Thickness of cylindrical shell
I : Mass inertia
L : Length of cylindrical shell
m : Number of axial half-waves
N : Number of circumferential waves
$\bar{N}_0$: Nondimensional axial load
N_0 , N_a : Axial load
N_{0cr} : Critical buckling load
r, θ, z : Radial, circumferential and transverse direction
R : Mean radius of cylindrical shell
u, v, w : Radial, circumferential, and transverse displacements
Ω : Nondimensional fundamental frequencies
κ : Shear correction factor
Φ : Volume fraction exponent
λ : Nondimensional natural frequency
ε_i , κ_i : Membrane and bending strains
ϕ_1 , ϕ_2 : Rotations of a normal to the reference surface
ρ : Mass density
ν : Poisson's ratio
ω : Fundamental frequency

Subscripts:

m,c : Metal & ceramic
eff : Effective

References

[1] M. Koizumi and M. Niino, Overview of FGM research in Japan, *MRS Bull*. 20 (1995) 19-21.
[2] J. N. Reddy, *Mechanics of Laminated Composite Plates and Shells*, Second Edition, CRC Press, New York (2004).
[3] J. N. Reddy and C. D. Chin, Thermomechanical Analysis of Functionally Graded Cylinders and Plates, *J. Thermal Stresses,* 26 (1) (1998) 593-626.
[4] R. A. Arciniega and J. N. Reddy, Large deformation analysis of functionally graded shells, *Int. J. Solid Struct.* 44 (2007) 2036-2052.
[5] G. N. Praveen, C. D. Chin and J. N. Reddy, Thermoelastic Analysis of a Functionally Graded Ceramic-Metal Cylinder, *ASCE J. Eng. Mech*. 125 (11) (1999) 1259-1267.
[6] C. T. Loy, K. Y. Lam and J. N. Reddy, Vibration of functionally graded cylindrical shells, *Int. J. Mech. Sciences*, 41 (1999) 309-24.
[7] S. C. Pradhan, C. T. Loy, K. Y. Lam and J. N. Reddy, Vibration characteristics of functionally graded cylindrical shells under various boundary conditions, *Appl. Acoust*. 61 (2000) 119-129.
[8] S. W. Gong, K. Y. Lam and J. N. Reddy, The elastic response of functionally graded cylindrical shells to low-velocity impact, *Int. J. Imp. Eng*. 22 (1999) 397-417.
[9] T. Y. Ng, K. M Lam, K. M. Liew and J. N. Reddy, Dynamic stability analysis of functionally graded cylindrical shells under periodic axial loading, *Int. J. Solid Struct.* 38 (2001) 1295-309.
[10] A. H. Sofiyev, The stability of compositionally graded ceramic–metal cylindrical shells under a periodic axial impulsive loading, *Compos. Struct.* 69 (2005) 247-257.
[11] M. Darabi, M. Darvizeh and A. Darvizeh, Non-linear analysis of dynamic stability for functionally graded cylindrical shells under periodic axial loading, *Compos. Struct*. 83 (2) (2008) 201-211.
[12] H. Matsunaga, Free vibration and stability of functionally graded circular cylindrical shells according to a 2D higher order deformation theory, *Compos. Struct*. 88 (4) (2009) 519-531.
[13] H. Matsunaga, Free vibration and stability of functionally graded shallow shells according to a 2D higher-order deformation theory, *Compos. Struct*. 84 (2) (2008) 132-146.
[14] S. P. Timoshenko and S. Woinowsky-Krieger, *Theory of Plates and Shells*, 2nd Edition, McGraw-Hill, New York (1959).
[15] V. V. Bolotin, *The Dynamic Stability of Elastic Systems*, Holden-Day, San Francisco (1964).

Appendix A

$$T_{11} = A_{11}\lambda_m^2 + \frac{A_{66}n^2}{R^2} \qquad T_{12} = -\frac{A_{12}+A_{66}}{R}\lambda_m n$$

$$T_{13} = -\frac{A_{12}}{R}\lambda_m \qquad T_{14} = B_{66}\lambda_m^2 + \frac{B_{66}n^2}{R^2}$$

$$T_{15} = -\frac{B_{12}+B_{66}}{R}\lambda_m n \qquad T_{21} = -\frac{A_{12}+A_{66}}{R}\lambda_m n$$

$$T_{22} = A_{66}\lambda_m^2 + \frac{A_{22}n^2}{R^2} + \frac{C_{55}}{R^2} \qquad T_{23} = \frac{A_{22}+C_{55}}{R}n$$

$$T_{24} = -\frac{B_{21}+B_{66}}{R}\lambda_m n \qquad T_{25} = B_{66}\lambda_m^2 + \frac{B_{22}n^2}{R^2} - \frac{C_{55}}{R^2}$$

$$T_{31} = -\frac{A_{21}}{R}\lambda_m \qquad T_{32} = \frac{C_{55} + A_{22}}{R^2} n$$

$$T_{33} = C_{44}\lambda_m^2 + \frac{C_{55}n^2}{R^2} + \frac{A_{22}}{R^2} \qquad T_{34} = \left(C_{44} - \frac{B_{21}}{R}\right)\lambda_m$$

$$T_{35} = -\frac{C_{55}R - B_{22}}{R^2} n \qquad T_{41} = B_{11}\lambda_m^2 + \frac{B_{66}n^2}{R^2}$$

$$T_{42} = -\frac{B_{12} + B_{66}}{R}\lambda_m n \qquad T_{43} = \left(C_{44} - \frac{B_{12}}{R}\right)\lambda_m$$

$$T_{44} = D_{11}\lambda_m^2 + \frac{D_{66}n^2}{R^2} + C_{44} \qquad T_{45} = -\frac{D_{12} + D_{66}}{R}\lambda_m n$$

$$T_{51} = -\frac{B_{21} + B_{66}}{R}\lambda_m n \qquad T_{52} = B_{66}\lambda_m^2 + \frac{B_{22}n^2}{R^2} - \frac{C_{55}}{R}$$

$$T_{53} = \frac{B_{22} - RC_{55}}{R^2} n \qquad T_{55} = \frac{D_{22}}{R^2} n^2 + C_{55} + \frac{D_{66}}{R}\lambda_m^2$$

$$T_{54} = -\frac{D_{21}}{R}\lambda_m n - \frac{D_{66}}{R}\lambda_m n$$

Farzad Ebrahimi received his B.S., M.S. and his PhD in Mechanical Engineering from the University of Tehran, Iran. His PhD research was under the title of "Vibration analysis of smart functionally graded plates" at the Smart Materials and Structures Lab in the Faculty of Mechanical Engineering of the University of Tehran. His research interests include vibration analysis of plates and shells, smart materials and structures and functionally graded materials.